THE EFFECT OF MULTIPLE WELD REPAIRS ON THE FATIGUE RESISTANCE OF WELDED ALUMINUM ALLOY 5083-O

John R. Panico

NAVAL POSTGRADUATE SCHOOL
Monterey, California

THESIS

The Effect Of Multiple Weld Repairs
On The Fatigue Resistance Of
Welded Aluminum Alloy 5083-0

by

John R. Panico

December 1979

Thesis Advisor T.R. McNelley

Approved For Public Release; Distribution Unlimited

UNCLASSIFIED

SECURITY CLASSIFICATION OF THIS PAGE (When Data Entered)

REPORT DOCUMENTATION PAGE		READ INSTRUCTIONS BEFORE COMPLETING FORM
1. REPORT NUMBER	2. GOVT ACCESSION NO.	3. RECIPIENT'S CATALOG NUMBER
4. TITLE (and Subtitle) The Effect Of Multiple Weld Repairs On The Fatigue Resistance Of Welded Aluminum Alloy 5083-0		5. TYPE OF REPORT & PERIOD COVERED Master's Thesis December 1979
		6. PERFORMING ORG. REPORT NUMBER
7. AUTHOR(s) John R. Panico		8. CONTRACT OR GRANT NUMBER(s)
9. PERFORMING ORGANIZATION NAME AND ADDRESS Naval Postgraduate School Monterey, California 93940		10. PROGRAM ELEMENT, PROJECT, TASK AREA & WORK UNIT NUMBERS
11. CONTROLLING OFFICE NAME AND ADDRESS Naval Postgraduate School Monterey, California 93940		12. REPORT DATE
		13. NUMBER OF PAGES 58
14. MONITORING AGENCY NAME & ADDRESS(if different from Controlling Office)		15. SECURITY CLASS. (of this report)
		15a. DECLASSIFICATION/DOWNGRADING SCHEDULE

16. DISTRIBUTION STATEMENT (of this Report)

Approved for public release; distribution unlimited.

17. DISTRIBUTION STATEMENT (of the abstract entered in Block 20, if different from Report)

18. SUPPLEMENTARY NOTES

19. KEY WORDS (Continue on reverse side if necessary and identify by block number)

Precipitate Agglomeration
Aluminum-Magnesium Alloy 5083-0
Fatigue Resistance
Liquified Natural Gas Applications
Weld Cycle Effects

20. ABSTRACT (Continue on reverse side if necessary and identify by block number)

This work follows that of Lt. G.R. Speight, USCG, on the general microstructural and mechanical property effects of multiple weld repairs in 5083-0 aluminum, and extends the previous study in to the area of fatigue. The essential observation made is that multiple weld repairs do not significantly affect the fatigue resistance of the material. Microstructural changes in the base metal do not alter crack

DD FORM 1 JAN 73 1473 EDITION OF 1 NOV 65 IS OBSOLETE
S/N 0102-014-6601

(Page 1)

UNCLASSIFIED

SECURITY CLASSIFICATION OF THIS PAGE (When Data Entered)

initiation and propagation characteristics, failure being confined to the weld filler material.

Approved For Public Release; Distribution Unlimited

The Effect Of Multiple Weld Repairs On The Fatigue Resistance Of Welded Aluminum Alloy 5083-0

by

John R. Panico
Lieutenant Commander, United States Navy
B.S., United States Naval Academy, 1970

Submitted In Partial Fulfillment Of
The Requirements For The Degree Of

MASTER OF SCIENCE IN MECHANICAL ENGINEERING

from the

NAVAL POSTGRADUATE SCHOOL
December 1979

TABLE OF CONTENTS

ABSTRACT

This work follows that of Lt. G.R. Speight, USCG, on the general microstructural and mechanical property effects of multiple weld repairs in 5083-0 aluminum, and extends the previous study into the area of fatigue. The essential observation made is that multiple weld repairs do not significantly affect the fatigue resistance of the material. Microstructural changes in the base metal do not alter crack initiation and propagation characteristics, failure being confined to the weld filler material.

LIST OF FIGURES

7. The metallography specimen showing general dimensions. The indicated location array is shown to give the reader a general idea of the areas represented by micrographs.

8. Haversine Fatigue Test. Specimen loading as a function of time. A frequency of 10 hertz was used for all tests.

9. Photomicrographs taken of the as-polished specimen subjected to the original two-pass weld only. The locations represented are the interface (a), approximately 6 mm (b), 18 mm (c), and 27 mm (d) from the interface. (100X).

10. Photographs taken of the as-polished specimen subjected to 16 repair simulations. The locations represented are the interface (a), approximately 6 mm (b), 18 mm (c), and 27 mm (d) from the interface. (100X).

11. (a) Twice weld repaired specimen in the as-polished condition. Photograph taken on SEM. (2500X).

    (b) Fourteen weld repaired specimen in the as-polished condition. Photograph taken on the SEM. (2500X). It can be seen that the inclusions are coarsening and breaking up.

    (c) Fourteen weld repaired specimen in the as-polished condition. Photograph taken on the SEM. (7000X). Cracks have developed in the inclusions.

12. S-N Fatigue Diagram for AL 5083-0 original plate. σ_{MAX} on the haversine loading curve is plotted on the vertical axis while cycles to failure, N, is plotted on the horizontal axis.

13. S-N Fatigue Diagram for AL 5083-0 which has been weld repaired twice. σ_{MAX} on the haversine loading curve is plotted on the vertical axis while cycles to failure, N, is plotted on the horizontal axis.

14. S-N Fatigue Diagram for AL 5083-0 which has been weld repaired fourteen times. σ_{MAX} on the haversine loading curve is plotted on the vertical axis while cycles to failure, N, is plotted on the horizontal axis.

15. Comparative S-N Fatigue Diagram with Al 5083-0 original plate, two weld repaired Al 5083-0 alloy and fourteen weld repaired Al 5083-0 alloy plotted. σ_{MAX} on the haversine loading curve is plotted on the vertical axis while cycles to failure, N, is plotted on the horizontal axis.

16. Observation of the fracture surface of a twice weld repaired specimen. (240X). The fracture appears to have initiated at porosity near the surface. Radial fatigue striations mark the progress of the fatigue crack growth.

17. Observation of the fracture surface of a fourteen weld repaired sample. (620X). Porosity in the ductile overload zone is shown.

18. Observation of the fracture surface of a sample from the unwelded original plate. (25X). The fatigue crack seems to have begun at the free surface of the material and propagated inward.

19. The fatigue zone of Figure 18 at a magnification of 51 diameters.

20. Observation of transverse section of the fracture surface. (100X). The specimen is from an original plate. Note the absence of porosity.

21. Observation of transverse section of the fracture surface of a fourteen weld repaired sample. (100X). Note the porosity at or near the fracture surface. This observation along with that in Figure 12 indicate that the fatigue fracture in all welded samples was probably initiated at porosity located in the weld filler metal.

22. Observation of the entire fracture surface of a fourteen weld-repaired sample. (24X). A very large ductile overload zone and porosity are apparent.

LIST OF TABLES

ACKNOWLEDGEMENT

The author wishes to express his thanks to Professor Terry McNelley for his enthusiastic assistance and guidance throughout the course of this study. Numerous consultations with Mr. Tom Kellog, Mechanical Engineering Department Technician, were of invaluable assistance in solving problems encountered in specimen preparation and photography. The author extends special thanks to his wife, Judy, and daughter, Kristen, for their patience and understanding during the completion of this manuscript. Professor Kenneth Challenger's timely assistance was also greatly appreciated.

I. INTRODUCTION AND BACKGROUND

A. ALUMINUM LIQUIFIED NATURAL GAS (LNG) TANKS

The aluminum alloy 5083-0 is extensively used in marine applications. Its corrosion resistance, strength and weldability make it an excellent material for these applications. This alloy is used in two of the three major designs for LNG tankships. The material's light weight and resistance to fracture at low temperature are the primary material properties which make it especially suitable for LNG use. Further, it is non-sparking, an extremely desirable characteristic in marine transport of flammable material.

The three major designs are [1]: (1) the TECHNIGAZ membrane containment system, utilizing a stainless steel primary barrier, (2) the Moss-Rossenburg design spherical containment system, and (3) the Conch design prismatic containment system. The latter two systems utilize 5083-0 aluminum as the primary barrier. Since the purpose of this thesis is to determine the effects of multiple weld repairs on aluminum welded joints, discussion will be limited to designs (2) and (3). An LNG tanker of 125,000 m^3 capacity contains five separate tanks. When utilizing a self-supporting containment system, the tanks are fabricated independently of the vessel's hull and are not inserted into the hull until both the hull and tanks are complete (Figure 1). An important advantage of the self-supporting class system is that tank

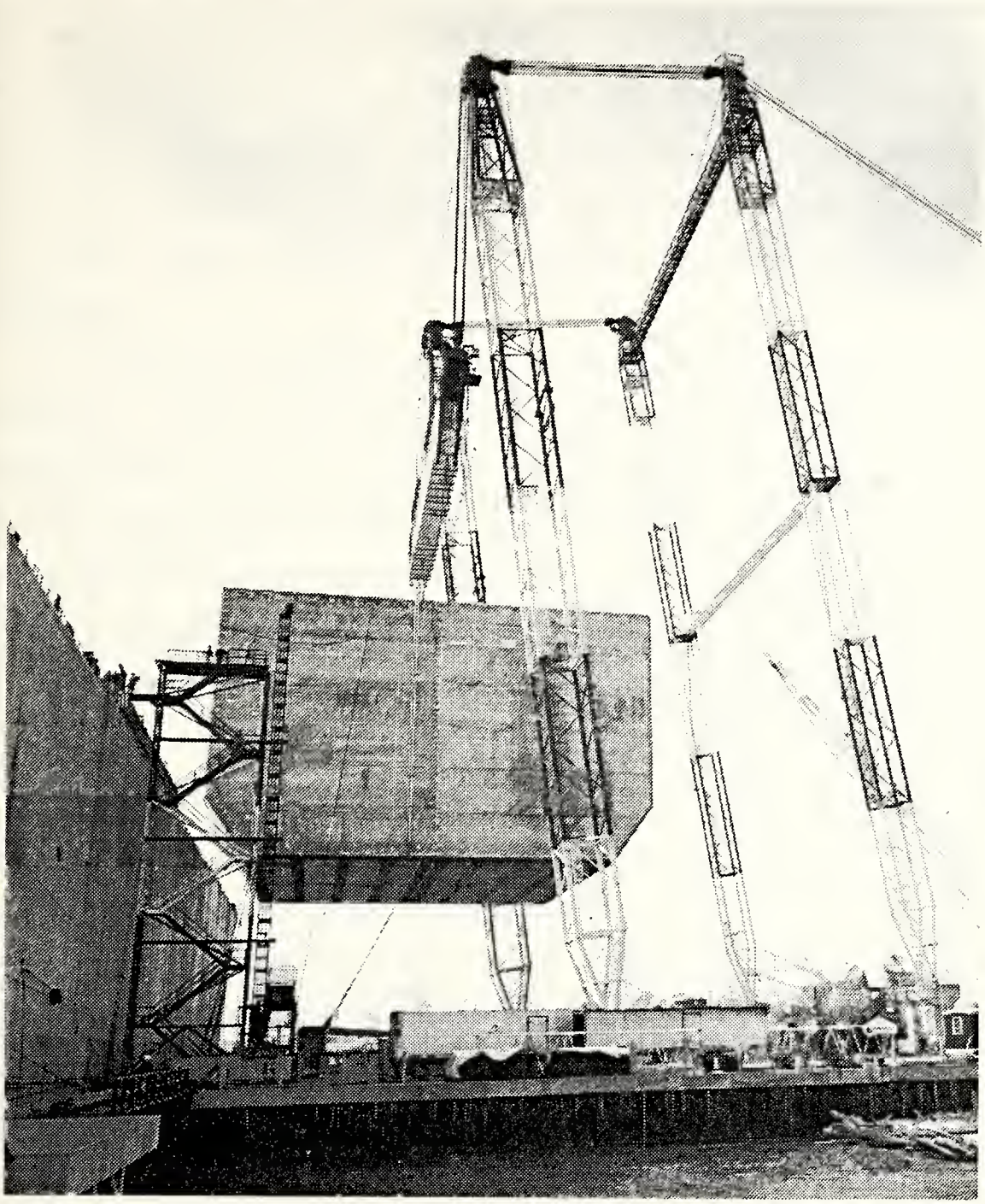

Figure 1. Photograph of a Conch design "self-supporting" Liquified Natural Gas tank being loaded aboard ship at the Kaiser Fabricators Facility, Mobile, Alabama. The tank, one of five to be placed in the ship, is of all-welded, 5083-0 aluminum construction. (Photograph compliments of Kaiser Aluminum Chemical & Sales Inc.)

construction may proceed independently of hull construction. This allows the tanks to be fabricated in controlled environments more advantageous for their specific fabrication requirements. A disadvantage in this design is the requirement for heavy lift capabilities to move and insert the tanks into the hulls. Here, aluminum's light weight becomes especially important.

In order to transport natural gas economically it must be liquified. The liquid natural gas is loaded aboard ship at a temperature of -165°C. This cryogenic temperature dictates that the containment vessel be constructed of material with sufficient low temperature toughness. Aluminum does not exhibit a ductile to brittle transition at low temperatures whereas ferritic and martensitic steels do. In fact, the strength of aluminum actually is higher at low temperatures and there is little loss in ductility in comparison to room temperature. Because of the hazardous nature of this cargo, the Coast Guard has imposed stringent code standards for weld quality. If a weldment in a LNG tank is determined to be defective by X-ray inspection it must be repaired. This weld repair consists of grinding out the old weld and rewelding the defective section. Frequently, multiple weld repairs are required in certain areas of a tank. It became apparent to the Coast Guard that their insistence on weld quality and the resultant weld repairing was subjecting the base metal in the tanks to severe temperature cycles due to the repeated application of the heat of welding. This problem then became the impetus for research in this area.

In the fall of 1978, Lt. George R. Speight Jr., USCG, conducted research in the areas of microstructural and mechanical properties of welded aluminum alloy 5803-0. He investigated the effect of multiple weld repairs on strength, hardness and stress corrosion cracking susceptibility. His results are summarized in Ref. 2. In general, his conclusions were that there is no pronounced effect on those properties, but a slight tendency toward degradation in these properties was observed. In particular, Speight noted rather pronounced microstructural effects in the heat affected zone of the base metal. Insoluble inclusions of $(FeMn)_3$ $SiAl_{12}$, and Mg_2Si (Ref. 3) appeared to coarsen with increasing numbers of weld repairs. In the present research, it was further noted that these coarsened inclusions also became internally fractured. The effect of this inclusion growth and fracturing on the fatigue resistance of weld repaired aluminum alloy 5083-0 was the subject of this thesis.

B. ALUMINUM-MAGNESIUM ALLOYS

The 5000 series aluminum-magnesium alloys are moderate in strength, allowing fabrication into large structures without excessive plate thickness and the attendant weight penalty. Further, the density of the aluminum-magnesium alloys such as 5083-0 is only one-third that of stainless steel. Since the strength of this alloy is approximately two-thirds that of stainless steel a substantial weight savings is obtained.

Thus, aluminum alloys are prime candidates for large structures which require lifting such as "self-supporting"

LNG containment systems. In addition, aluminum is relatively low in cost and readily available.

The aluminum-magnesium alloys are non-heat treatable, solid-solution type alloys known as the 5000 series. Magnesium, whose atoms exist as substitutional solutes in the aluminum matrix, provides strengthening in this series.

The magnesium content in the 5000 series varies from 0.5 to 5.0 weight percent depending on the specific alloy. Aluminum alloy 5083-0 studied in this research, contains 4.0% to 4.9% magnesium as the primary alloy addition. Detailed alloy chemistry and mechanical property data are given in Table I. In the unwelded annealed condition, this alloy exhibits a minimum yield strength of 18,000 PSI, a minimum ultimate tensile strength of 40,000 PSI and 16% elongation in two inches. Magnesium is an effective strengthening agent when used by itself or in the presence of manganese. One may ask why not increase the amount of magnesium present to further increase the strength? Many of the 5000 series alloys were developed for marine applications which expose the material to rather severe corrosive environments. Because of such applications, care must be taken to formulate alloys for corrosion and stress corrosion resistance as well as strength.

Figure 2 illustrates the equilibrium binary phase diagram for the aluminum-rich range of the aluminum-magnesium system. The actual phase diagrams for specific alloys are quite complicated due to the presence of numerous other elements added to strengthen and stabilize the alloy. For the purpose of this

TABLE I

ALLOY CHEMISTRY AND MECHANICAL PROPERTIES OF AL 5083-0

Chemical Composition Limits of Wrought Aluminum Alloy 5083

Element	Weight Percent
Silicon	0.40 max.
Iron	0.40 max.
Copper	0.10 max.
Manganese	0.3 - 1.0
Magnesium	4.0 - 4.9
Chromium	0.05- 0.25
Zinc	0.25
Titanium	0.15
Others	
each	0.05 max.
total	0.15
Aluminum	Remainder

Typical Mechanical Properties of Aluminum Alloy 5083-0

Alloy and Temper	5083-0
Strength, ksi (MPa)	
Ultimate Tensile	42(289.6)
Yield	21(144.8)
Elongation Percent in 2 inches	16
Hardness, R_F	79
Ultimate Shear Strength, ksi (MPa)	25(172.4)
Fatigue Endurance Limit, ksi (MPa)	--
Modulus of Elasticity, ksi (MPa)	10.3(71.0)

discussion, however, the binary phase diagram will suffice. Also shown in the same figure is a schematic representation of a welded joint, showing peak temperatures experienced during welding relative to the phase diagram. It is apparent from the phase diagram that an alloy with 4.5% magnesium solid solution is metastable at room temperature. Higher magnesium alloys become more susceptible to uncontrolled precipitation of the intermetallic β phase (Al_3Mg_2) during welding thermal cycles and hence become sensitized to stress-corrosion. For this reason, the magnesium content is restricted.

C. THERMAL CYCLES IN THE WELDING OF 5083 ALUMINUM

5083-0 aluminum is readily welded by any number of processes [4]. As with any material however, a knowledge of metallurgical response of the material to repeated thermal cycles is necessary to guarantee the integrity of the welded joint.

The aluminum LNG containment systems are fabricated utilizing the gas-metal arc welding process, metal-inert gas technique (MIG), as the primary joining method. During the welding process the material is subjected to peak temperatures ranging up to the liquidus (660°C); the exact temperature depending on distance from the weld [5]. Figure 2 shows the temperature attained at various positions in the base metal and the associated location in the phase diagram. As is evident from this figure, areas of the welded plate experience temperatures representing each of the equilibrium phase regions for this alloy.

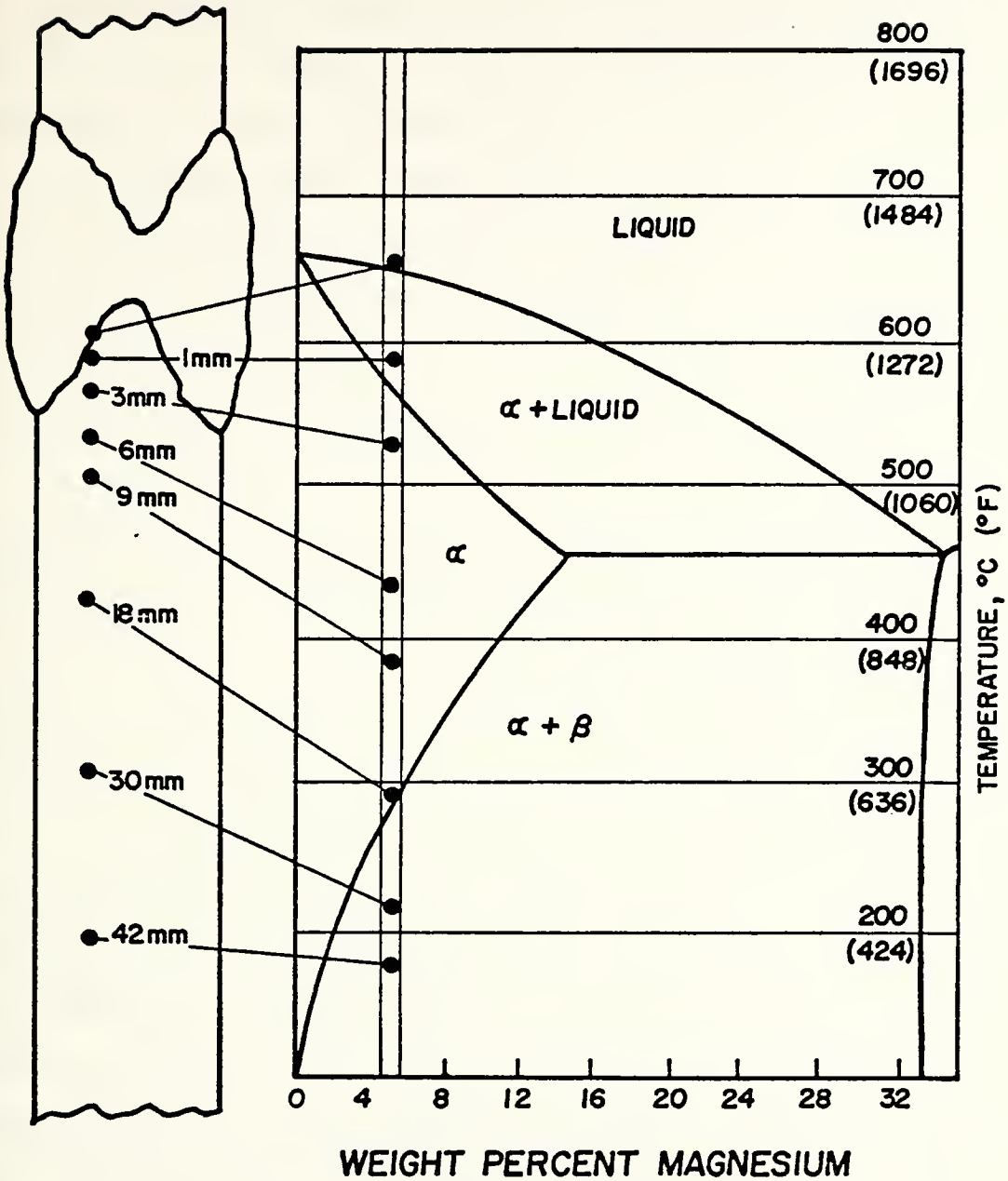

Figure 2. This figure represents the aluminum-magnesium binary equilibrium phase diagram. The defined vertical region is the percentage range of magnesium found in the 5083-0 alloy. The schematic of the welded joint is introduced to give the reader a general idea of the peak temperatures experienced at various distances from the weld interface relative to the phase diagram.

Another important point to consider is cooling rates experienced by the weldment during the welding process. Figure 3 illustrates three important facts:

(1) Peak temperatures experienced decrease at increased distances from the center of the weld.

(2) Time to peak temperature increases at increased distances from the weld.

(3) The cooling rate decreases at increased distances from the weld.

Aluminum exhibits a high thermal conductivity and this is responsible for the steep temperature gradient shown in Figure 3.

The influence of increasing numbers of weld repairs is to increase the total time at temperature. Further, since β precipitation will occur during only the cooling portion of the cycle, an increasingly large number of cycles experienced will likely have more effect than a total equivalent time at temperature but in a single cycle only. Speight [2] discussed the coarsening of both inclusions and β -phase precipitates in terms of partial solutioning during heating followed by re-precipitation during subsequent cooling. Large inclusions and re-precipitation then, tend to grow at the expense of smaller ones in this process.

In addition to these metallurgical considerations, one must be aware of the stress (or strain) cycles the material experiences during welding. As with any metal, aluminum undergoes thermal expansion and contraction with heating and cooling. Care must be taken to allow for these dimensional changes such

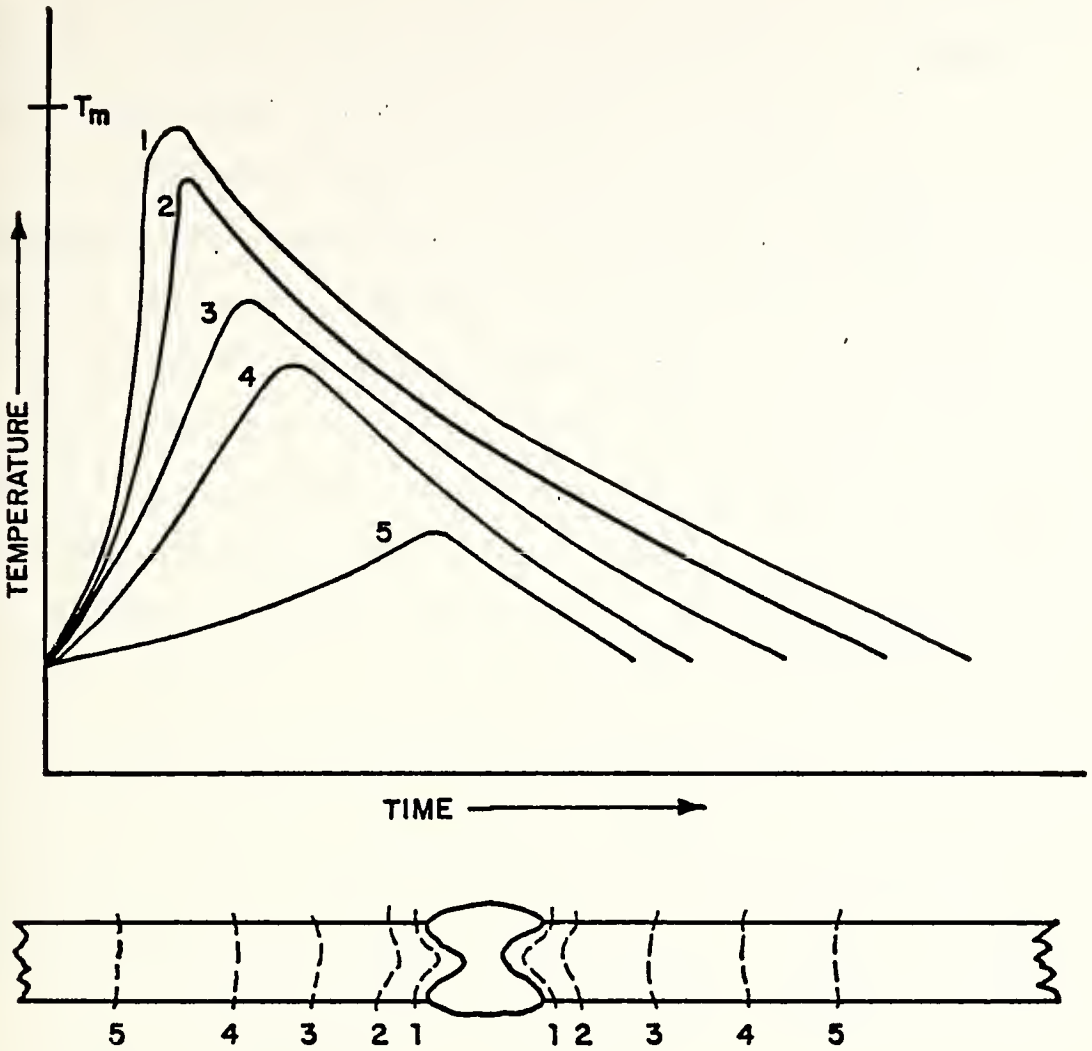

Figure 3. This figure shows curves which represent typical heating and cooling rates of a plate as a function of varying distances from the weld arc. The numbered curves correspond to the numbered locations shown on the schematic of the welded joint.

that the material is not overly constrained. Excessive mechanical constraint may lead to large amounts of plastic deformation and even fracture of the weld metal.

Many variables must be considered when attempting to determine peak temperatures and cooling rates experienced by metals being welded. The more important ones are: the density of the material, the plate temperature prior to welding, specific heat of the material and welding speed. Power input, and thus heat input, is a function of current density and electrode potential. The rate of conduction heat transfer is a function of the heat capacity, thickness, density and pre-weld temperature of the material being welded. These variables may be combined into a linear formula relating each of these to the peak temperatures experienced at a specific distance from the molten weld pool. This relationship, as found in Ref. 3 as equation 3.1 is:

$$\frac{1}{T_p - T_o} = \frac{4.13\rho CtY}{H_{NET}} + \frac{1}{T_M - T_O}$$

Where T_p is the peak or maximum temperature (^oC) at a distance Y (mm) from the weld interface, T_O is the uniform temperature (^oC) of the plate prior to welding, T_M is the melting temperature (^oC) of the metal being welded, H_{NET} is the net energy input which is further given by FEI/V, where E and I are the electrode potential (volts), and current (amps) respectively, F is the heat transfer efficiency and V is the travel speed (mm/s) of the arc. The density of the

material being welded ($g/_{mm}3$) is ρ, C is the specific heat of the solid metal being welded ($J/_{g}{}^{o}C$), and t is the thickness of the plate being welded (mm).

D. FATIGUE

Fatigue is a fracture mechanism where failure doesn't occur when the component is initially loaded; instead failure occurs after a number of load fluctuations have been experienced. Normally, failure begins with initiation of a small microcrack at the surface which then grows across a section, by incrementally increasing in length with each loading cycle, eventually leading to final fracture.

A macroscopic examination of fatigue fracture surface generally reveals a flat fracture surface. This indicates an absence of any appreciable amount of gross (macroscopic) plastic deformation during fatigue [6]. Often, when failure occurs over a long period of time, the fracture surface contains "beach markings". These lines can be attributed to different periods of crack extension.

In testing for fatigue, scatter in test results is common. There are numerous reasons for this scatter [8]. They include variations in testing environment, preparation on specimen surfaces, alignment of the test machine and a number of metallurgical variables. All data from this study was analyzed by regression analysis.

The fatigue behavior of nonferrous alloys is characterized by the lack of a "fatigue limit". A fatigue limit is the stress

value on an S-N diagram below which failure does not occur. The S-N diagram is a plot of fatigue stress plotted versus number of cycles to failure. Therefore, the "fatigue limit" for aluminum alloys has to be arbitrarily defined as some specific cyclic life usually ten million cycles.

Fatigue behavior is sensitive to alloy chemistry. Large inclusions can serve as potential crack nucleation sites and are therefore undesirable. Fatigue crack nucleation models generally describe the process as follows: [7]

(1) As a result of plastic straining, slip is produced.

(2) Slip bands of highly localized deformation are generated.

(3) At the surface, extrusions appear which penetrate along the length of the slip band and become sharp fissures.

(4) The fissure breaks through the matrix and a crack is formed.

In general fatigue can commonly be divided into the crack initiation period and the crack growth period. The concern of this research was to determine if the large, cracked inclusions developed in the HAZ of the base metal due to multiple weld repairs, would provide the crack initiation site. If this were the case, the crack initiation phase would have been skipped.

II. OBJECTIVES, PLANS AND PROCEDURES

A. OBJECTIVE

Multiple weld repairs are often required in certain areas of LNG tanks during their construction. The objective of this research was to simulate and then characterize the effect of multiple weld repairs on welded joints made in 5083-0 aluminum. In particular, this thesis studies the effect of these weld repairs on the fatigue resistance of the welded alloy 5083-0.

B. PLAN OF APPROACH

To meet the objectives outlined above, this research was conducted in three parts:

(1) Effects of multiple weld repairs on microstructure.

(2) Effect of multiple weld repairs on fatigue resistance.

(3) Fractography of failed samples.

The procedures followed, results and conclusions derived in each of these parts will be discussed in the remainder of this thesis.

C. SOURCE OF MATERIALS

Although this information is contained in Lt. G.R. Speight's work [2] it is added here to enhance the reader's understanding of the experiment. The weldments used in this investigation were obtained from the Kaiser Aluminum And Chemicals Inc., Center For Technology, Pleasonton, California. The simulation of multiple weld repairs was performed under laboratory conditions to preclude the introduction of additional variables.

So that a proper correlation could be made between these tests and actual structures it was, however, desirable to duplicate industrial welding practice and materials as closely as possible. Thus it was necessary to acquire material of the proper alloy and temper. Due to cost constraints and material availability, 5083 aluminum alloy in the H-321 temper (cold worked rather than annealed) was purchased. This material was then annealed to produce to "0" temper; this anneal consisted of a controlled heating to 454^{o}C, followed by a two hour soak at temperature and a controlled furnace cool-down cycle. The welding, or filler, wire used in fabrication of the test plates was of 5183 type, identical to that used in the fabrication of the LNG tanks.

D. PROCEDURES

The various procedures used in this study approximate standard industrial practices and tests as closely as possible. Details regarding specimen preparation and the individual tests are discussed in the following sections.

1. Welding Of The Test Plates

The plates to be welded were all cut from the same rolled plate. Each plate was cut so that its greatest dimension was oriented in the direction of rolling. The plates to be welded measured approximately 254 x 610 x 12.7 millimeters (10 x 24 x 0.5 inches). The plates were then annealed as described above to the "0" temper. All plates were then degreased with acetone. A 30^{o} bevel weld preparation was machined on one side of each plate as shown in Figure 4(a). After the plates were welded on one side in the flat (down-hand) position they were

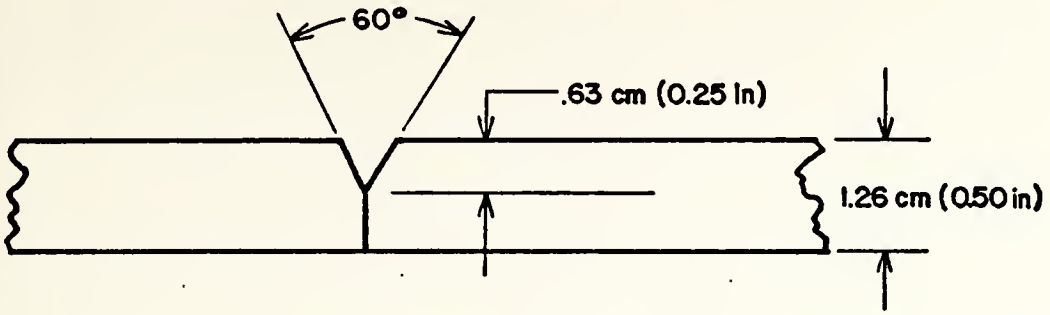

Figure 4 (a)

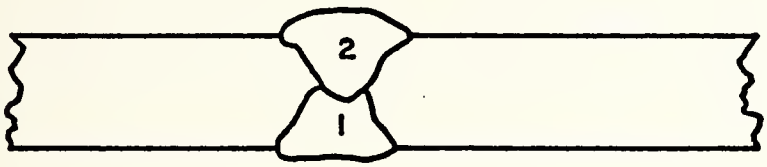

Figure 4 (b)

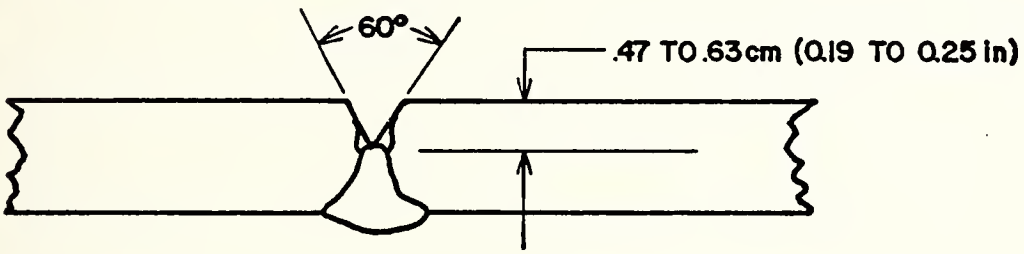

Figure 4 (c)

Figure 4 . (a) This figure represents the joint preparation performed prior to laying the first "downhand" or "flat" weld bead. After the first pass the plate is allowed to cool to a specified interpass temperature of 66°C (150°F) or less. The reverse side is backmilled to a minimum depth of 4.8 mm (3/16 inch) and then welded in the "flat" position.

(b) The overlapping roots of the two passes.

(c) The subsequent repair welds are made by grooving as shown, cooling to the temperature indicated above, and welding. The repair welds are made in a "flat" mode by changing plate sides with each single pass repair.

turned over, backmilled (included angle of 60°) and again welded in the flat position, Figure 4(b). A total of nine plates were welded in this fashion. One of the nine plates was set aside as a control sample, i.e., no weld repair. The remaining eight plates were subjected to weld repair simulations. Each repair simulation was performed by welding after remachining as shown in Figure 4(c). The first of the remaining eight plates was subjected to this repair simulation twice, first on one side then on the other with each weld being performed in the flat position. The second plate underwent four repair simulations (two repairs on each side). Plates three through eight underwent a progression of six through sixteen repair simulations, respectively, with an equal number of weld repairs on each side. The original and simulated repair welds were made by the Automatic Gas Metal Arc Process, Metal Inert Gas Technique, utilizing the welding parameters as shown in Table II.

After welding, the test plates were radiographed and reviewed in accordance with procedures set forth in Section VIII Division 1 of the 1971 edition of the ASME Code. Thus assuring radiographic weld quality commensurate with those required for commercially built LNG tanks. The location of subsequent fatigue test specimens relative to the test plate were as shown in Figure 5.

2. Fatigue Specimen Preparation

Fatigue specimens were machined from the welded sample plate as illustrated in Figure 5. Care was taken to include both weld metal and the heat affected zone in the test section of the specimen.

TABLE II

WELDING PARAMETERS USED IN FABRICATION OF TEST PLATES

	ORIGINAL WELD & REPAIR WELD
WELDING PROCESS	Automatic Gas Metal Arc
ATMOSPHERE	75% Helium & 25% Argon shielding gas
SHIELDING GAS FLOW	80 Cubic feet per hour
NOZZLE OPENING DIAMETER	0.625 inches
TYPE POWER SOURCE	Drooping Characteristic
CURRENT TYPE	Direct Current Reverse Polarity
ELECTRODE POTENTIAL	Negative
BASE METAL	5083-0 Aluminum
BASE METAL THICKNESS	0.50 inch
FILLER METAL	5183 Aluminum
FILLER METAL DIAMETER	1/16 inch
WELDING POSITION	Downhand (Flat)
AMPERAGE	250-260 Amps
VOLTAGE	33-34 Volts
RATE OF WIRE FEED	395 inches per minute
MACHINE TRAVEL SPEED	18 to 22 inches per minute

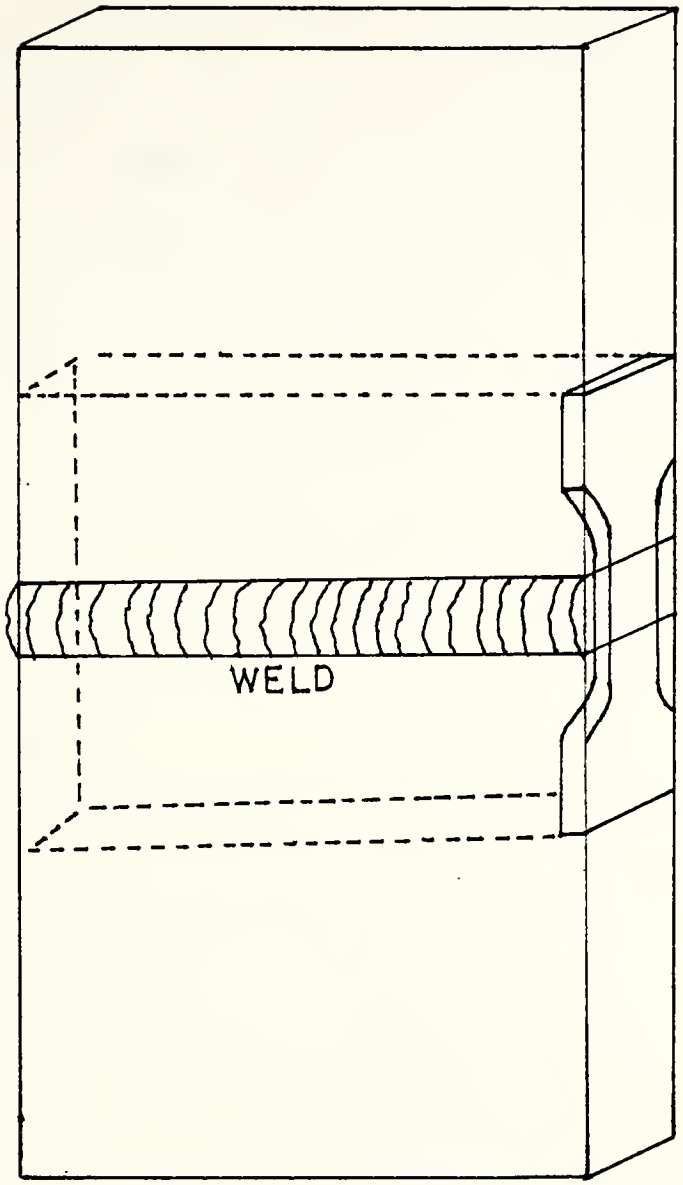

SPECIMEN ORIENTATION

Figure 5. Schematic representing the orientation of the sample in the welded plate. Both the weld metal and heat affected zone are included in the test section of the specimen.

An important consideration in the testing was whether the material failed in the base metal, heat affected zone (HAZ), or the weld material. Figure 6 is a representation of the finished fatigue specimens. All manufacturing of these specimens was done at the Intercity Machine Company in Seaside, California. A final polishing of the flat surfaces of the specimens was accomplished with the HANDIMET ® grinder, a wet sanding machine. Sequential sanding with abrasive paper of grit 240, 320, 400, and 600 was completed on each specimen prior to testing. This finishing removed milling marks and provided a final metal removal in a direction parallel to the long axis of the specimen in accordance with Ref. 9.

3. Microscopy

Microstructural comparisons were made in the as-polished condition utilizing both optical and Scanning Electron Microscopy (SEM). Specimens were machined and sectioned from the plate to the shapes shown in Figure 7. These specimens were used for both optical and Scanning Electron Microscope (SEM) microscopy. These then were mounted on 1-1/4 inch diameter stages for viewing in the Scanning Electron Microscope and examined in the locations indicated. Surface preparation was the same for both optical and SEM specimens. First, the specimens were ground using 0-grit silicon carbide paper. Then two rotating polishing wheels using aluminum oxide slurries of 0-grit and 15 m-grit were used. Finally, a rotating polishing wheel using MAGOMET magnesium oxide polishing compound was used to produce the final finish. Specimens were

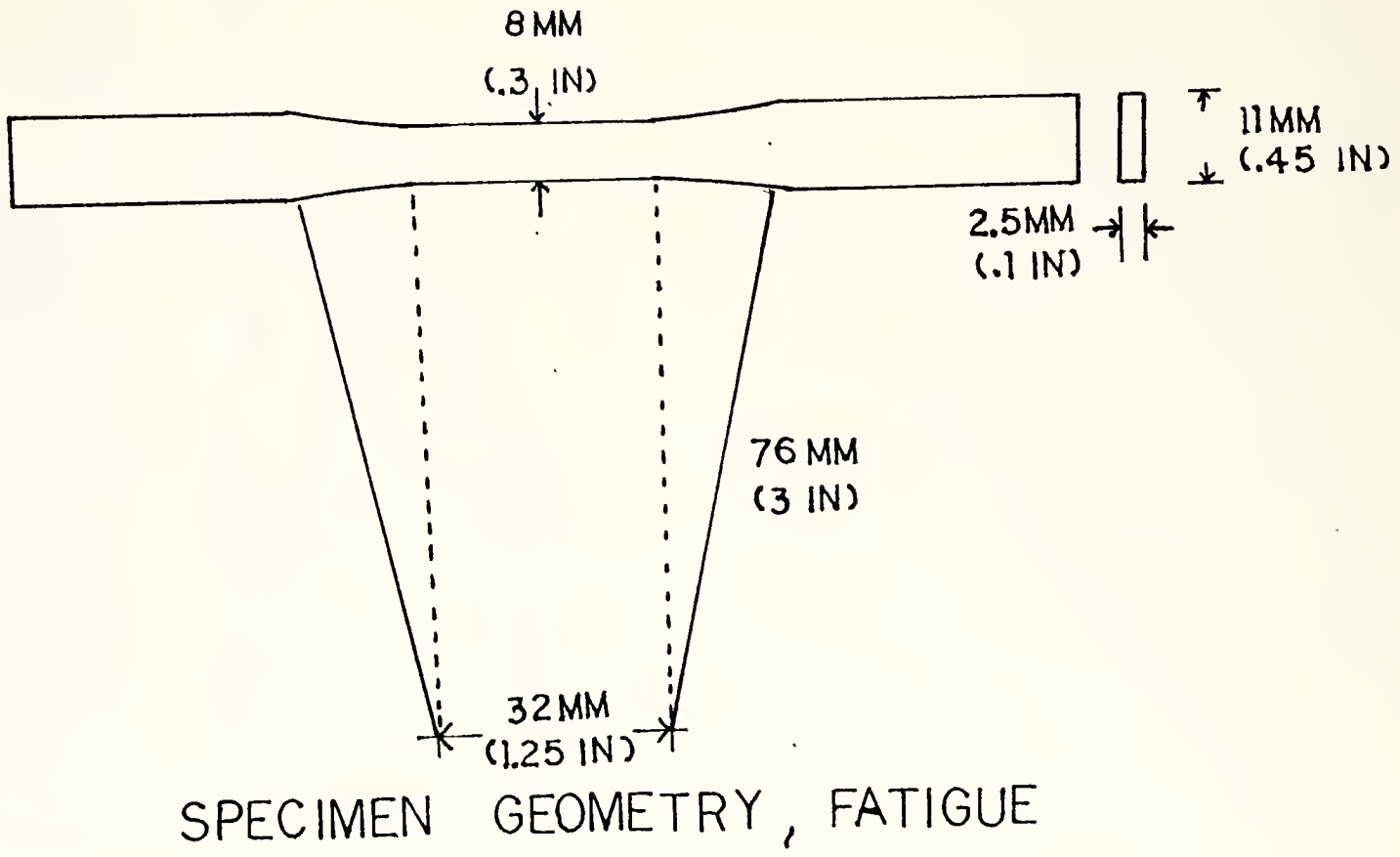

Figure 6. This figure represents the specimens used in fatique testing. The overall length of the specimen is 146 mm (5.75 in.).

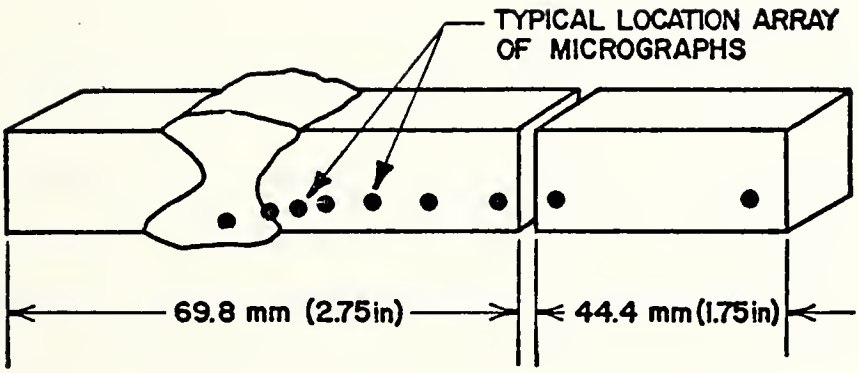

Figure 7. The metallography specimens showing general dimensions. The indicated location array is shown to give the reader a general idea of the areas represented by the micrographs.

rinsed with tap water and then by distilled water between each polishing stage. This polishing procedure was performed on each specimen prior to examination.

All optical microscopy was performed with the Bausch and Laumb Balpan Conference Microscope. All scanning electron microscopy was completed utilizing the Cambridge S4-10 Stereoscan Scanning Electron Microscope. Both microscopes are located in the microscope laboratory at the Naval Postgraduate School.

a. Microscopic Examination In The As-Polished Condition

Microscopic examination in the as-polished condition was performed on specimens from four, fourteen and sixteen repair simulations. These investigations were conducted to study differences in insoluble inclusions among the specimens.

b. Scanning Electron Microscopy In The As-Polished Condition

These investigations were conducted at magnifications ranging from 24X to 7000X. Differences in insoluble inclusions were studied as in the optical microscopy. Also, fractography of the broken fatigue specimens was conducted using this method.

4. Fatigue Testing

Fatigue testing was conducted on specimens taken from the plates corresponding to the original plate (no weldment) and plate with two weld repairs and fourteen repairs using the Series 810 Material Testing System located in basement of Halligan Hall at the Naval Postgraduate School.

The testing method followed the method developed by Krause, Landgraf, and Crandall of the Ford Motor Company [10].

In general it is a method to test thin guage specimens in fatigue. Because of the danger of buckling with fully reversible loading, a haversine tension-tension loading was employed. Figure 8 is a representation of the loading curve used in this thesis. A frequency of ten Hz was used for all tests.

The stress ratio, R, is the algebraic ratio of the minimum stress to the maximum stress. For comparability of results the stress ratio was maintained at R = .11 for all tests [11].

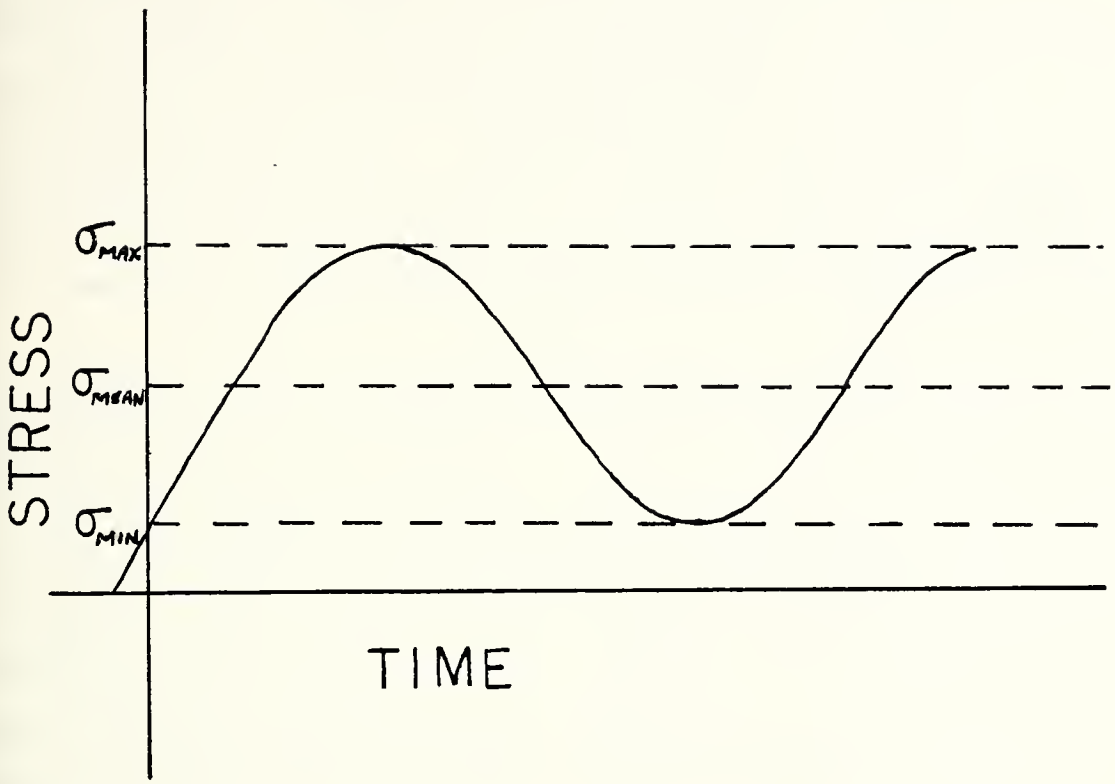

HAVERSINE FATIGUE TEST

Figure 8. Haversine Fatigue Test. Specimen loading as a function of time. A frequency of 10 hertz was used for all tests.

III RESULTS AND DISCUSSION

Lt. G.R. Speight's research in this area disclosed that the insoluble inclusions $(FeMn)_3 SiAl_{12}$ and Mg_2Si grew and coarsened with increasing numbers of weld repairs [27]. Figures 9 and 10 illustrate this coarsening. Figure 9 shows micrographs of an as-polished specimen subjected to the original two-pass weld only. Figure 10 shows micrographs of an as-polished specimen subjected to sixteen repair simulations. This coarsening had little apparent effect on tensile strength, stress corrosion cracking susceptibility and hardness, although, as noted previously, there was a slight tendency toward degradation in these properties.

The concern then focused on the effect of this coarsening and growth of the inclusions on the fatigue life of the welded and weld repaired alloy aluminum 5083-0. In 5083 aluminum weldments fatigue failure normally occurs in the weld filler material due to the presence of porosity and inclusions as a result of welding.

A. MICROSTRUCTURAL ANALYSIS

Microstructural examination was performed in the as-polished condition. Specific metallographic procedures were discussed in Section II.D. The results of such examination are given in the following paragraphs.

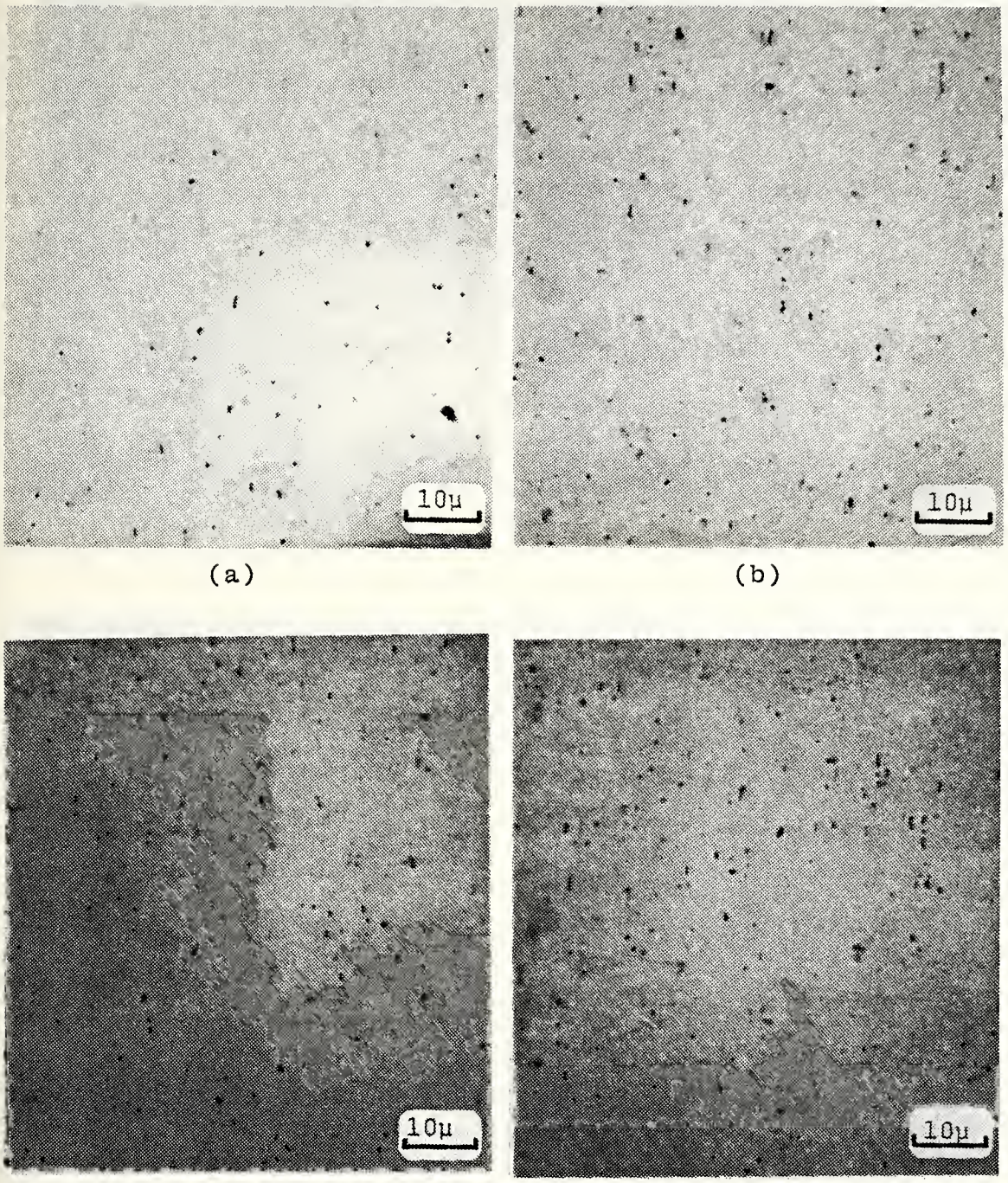

Figure 9. Photomicrographs taken of the "as-polished" specimen subjected to the original two-pass weld only. The locations represented are the interface (a), approximately 6 mm (b), 18 mm (c) and 27 mm (d) from the interface. (100X)

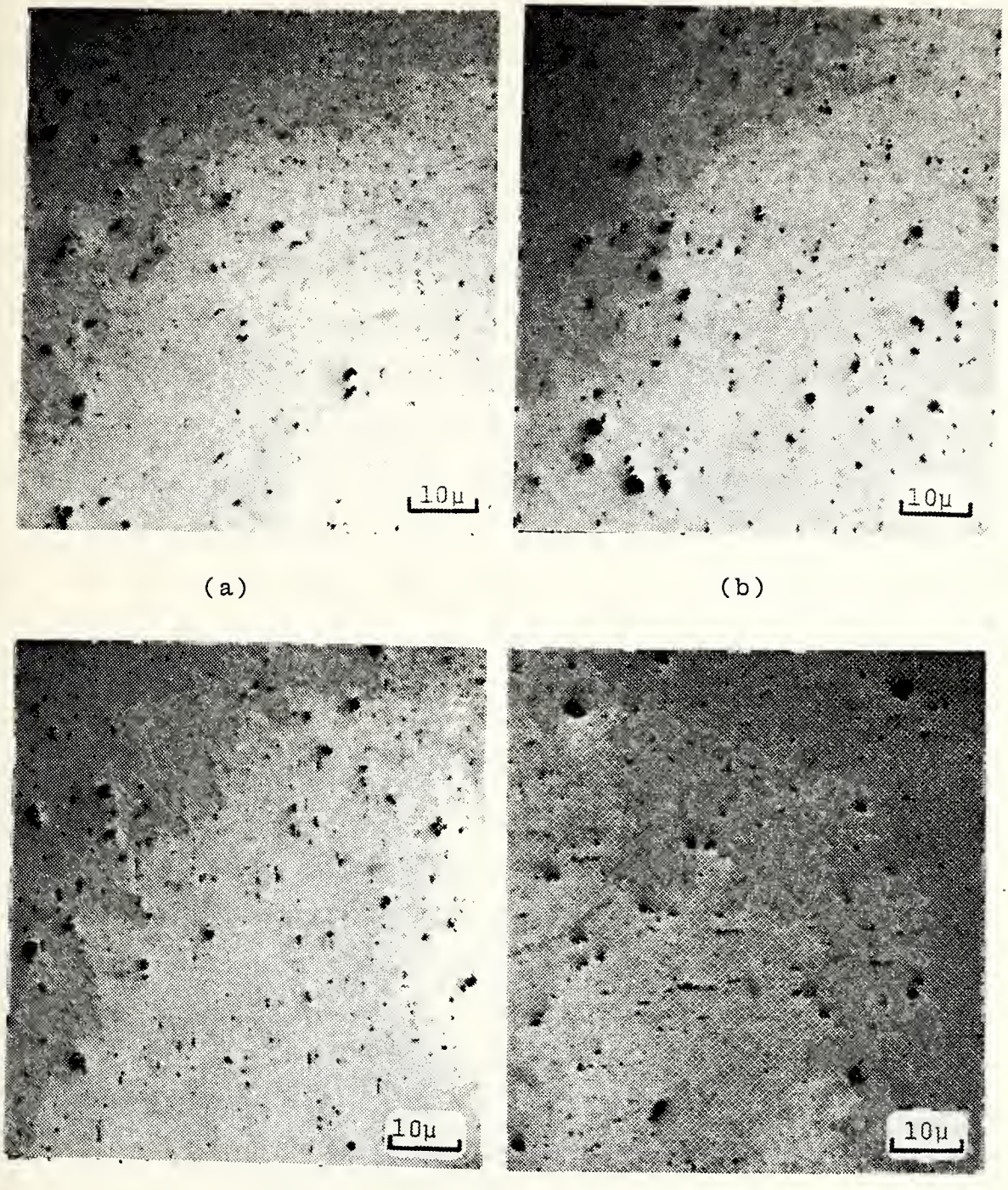

Figure 10. Photographs taken of the "as-polished" specimen subjected to 16 repair simulations. The locations represented are the interface (a), approximately 6 mm (b), 18 mm (c) and 27 mm (d) from the interface. (100X)

(1) Optical Microscopic Examination In The As-Polished Condition.

Summarized in Section II above. Figures 9 and 10 illustrate the microstructure.

(2) SEM Examination In The As-Polished Condition.

Closer examination was necessary to determine the effects of increasing numbers of weld repairs on the inclusions. Figure 11(a) shows a twice weld repaired specimen. Figure 11(b) was taken of a fourteen weld repaired sample. Note how the inclusions have broken up and although not evident in this figure, generally the included particles coarsened. Figure 11(c) is a photograph of an inclusion in a fourteen weld repaired sample at a magnification of 7000X. Note that cracks are clearly evident in the inclusion. This then was the question: Given the coarsening and cracking of insoluble inclusions in the HAZ, would these inclusions serve as crack initiation sites and lead to a change in the fracture location from the weld metal to the HAZ, resulting in a reduction of fatigue life.

B. FATIGUE RESULTS

Fatigue testing was performed to determine fatigue strength as a function of number of weld repair simulations. Graphical representation of fatigue data are shown in Figures 12 through 15. Also, the fatigue data are tabulated in Table III. The results of the fatigue tests are discussed below.

Fatigue testing was performed on specimens from the original plate, a twice weld repaired plate and a fourteen weld repaired

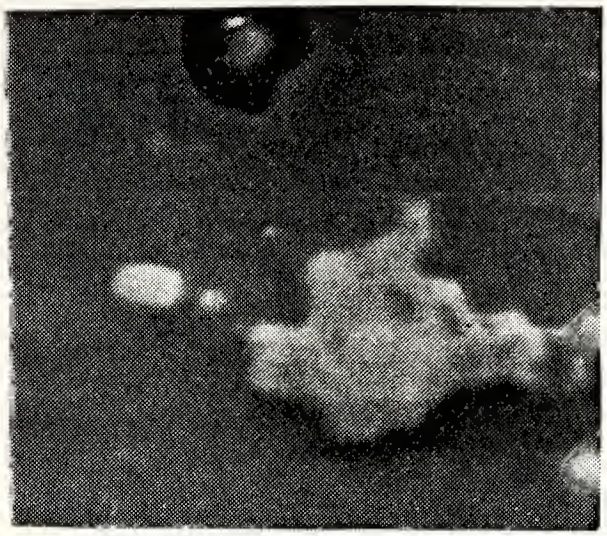

Figure 11 (a). Twice weld repaired specimen in the as-polished condition. Photograph taken on SEM. (2500X).

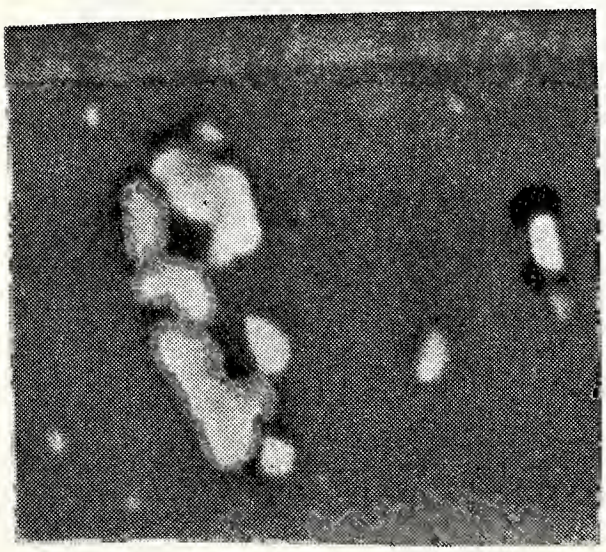

Figure 11 (b). Fourteen weld repaired specimen in the as-polished condition. Photograph taken on the SEM. (2500X). It can be seen that the inclusions are coarsening and breaking up.

Figure 11 (c). Fourteen weld repaired specimen in the as-polished condition. Photograph taken on the SEM. (7000X). Cracks have developed in the inclusions.

TABLE III

FATIGUE TEST DATA - AL 5083-0 ORIGINAL PLATE

SPECIMEN #	FREQUENCY (HERTZ)	STRESS (σ_{MAX}) (PSI)	CYCLES TO FAILURE
2A(1)	10	24,750	604,300
2A(2)	10	26,230	447,000
2A(3)	10	30,000	327,800
2A(4)	10	29,902	181,200
2A(5)	10	32,219	171,400
2A(6)	10	33,475	112,500
2A(7)	10	36,503	77,700
2A(8)	10	37,081	44,000

FATIGUE TEST DATA - AL 5083-0 TWO WELDED REPAIRS

SPECIMEN #	FREQUENCY (HERTZ)	STRESS (σ_{MAX}) (PSI)	CYCLES TO FAILURE
2 (1)	10	23,873	876,200
2 (2)	10	27,426	557,500
2 (3)	10	30,098	208,000
2 (4)	10	32,219	95,100
2 (5)	10	36,503	55,900

TABLE III (CONTINUED)

FATIGUE TEST DATA - AL 5083-0 FOURTEEN WELD REPAIRS

SPECIMEN #	FREQUENCY (HERTZ)	STRESS ($\bar{\sigma}_{MAX}$) (PSI)	CYCLES TO FAILURE
10 (1)	10	23,954	536,100
10 (2)	10	27,425	292,800
10 (3)	10	30,098	156,400
10 (4)	10	32,219	90,600
10 (5)	10	36,503	51,000

plate. In Figures 12 through 15 a least squared regression analysis was used to produce the straight lines through the data points.

Figure 15 is a comparative graph which shows the relation of the three fatigue curves (original plate, two repairs, fourteen repairs). There is only a slight difference between the results of these tests, however there appears to be a slight decrease in the fatigue resistance of the fourteen weld repaired sample as compared to the original plate and the twice-repaired plate. It should also be noted that for maximum stresses above about 27000 PSI (186 MPA) the twice weld-repaired specimen appears to be stronger than the original plate, possibly due to scatter in the data.

It is most significant that all the weld-repaired samples failed in the weld area. This answers the question posed in Section III above. The fatigue crack initiation remained in the weld area. It did not shift into the HAZ as a result of coarsening and cracking of inclusions, induced by increasing numbers of weld repairs. This also explains the similarity between the S-N curves in Figure 15. Since the failure occurs in the weld it makes little if any difference how many times the material is weld repaired. Additionally, the similarity in the properties of the filler metal to that of the original plate explains the close correlation of the original plate fatigue data to the welded plate data for the conditions tested.

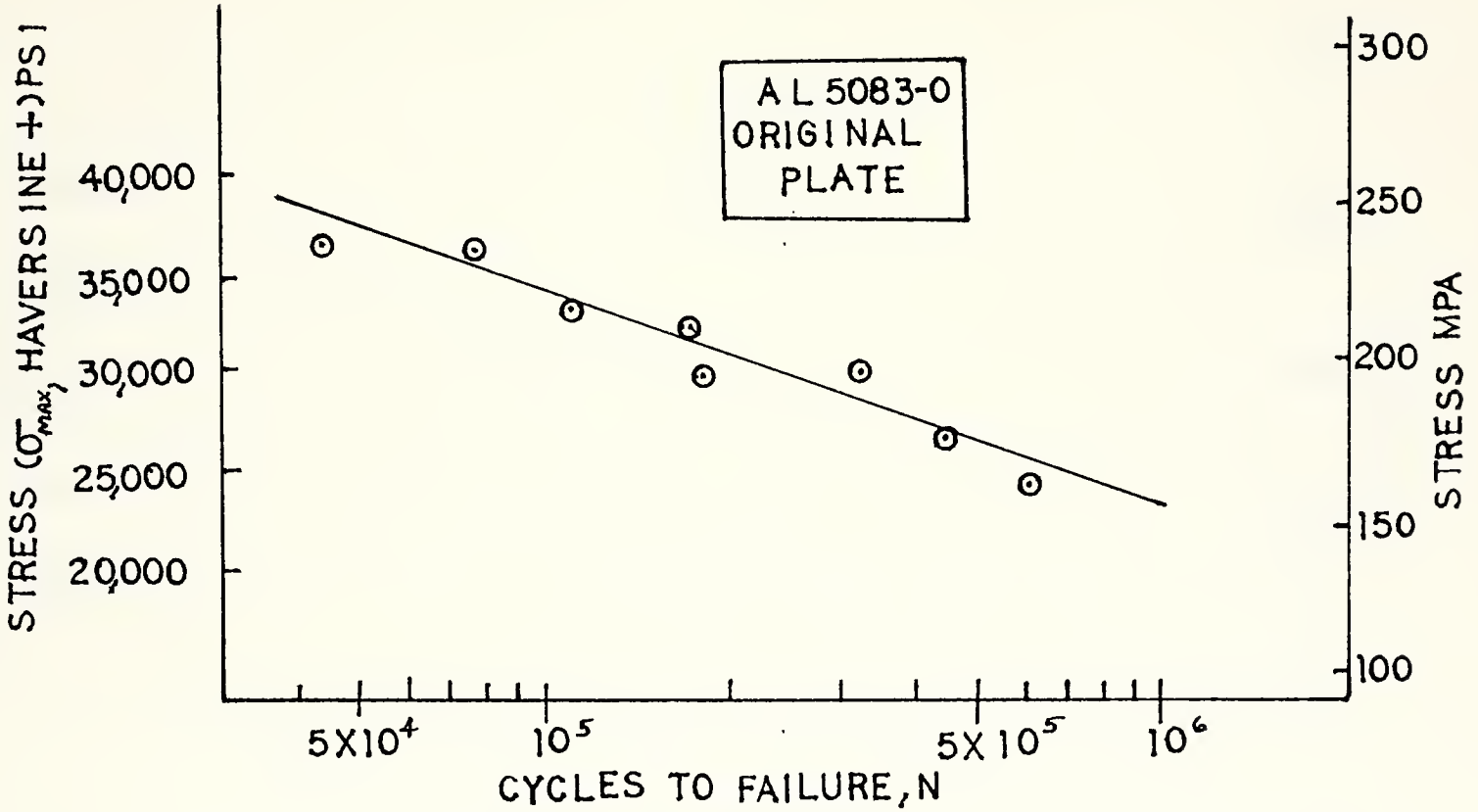

Figure 12. S-N Fatigue Diagram for AL 5083-0 original plate. σ_{MAX} on the haversine loading curve is plotted on the vertical axis while cycles to failure, N, is plotted on the horizontal axis.

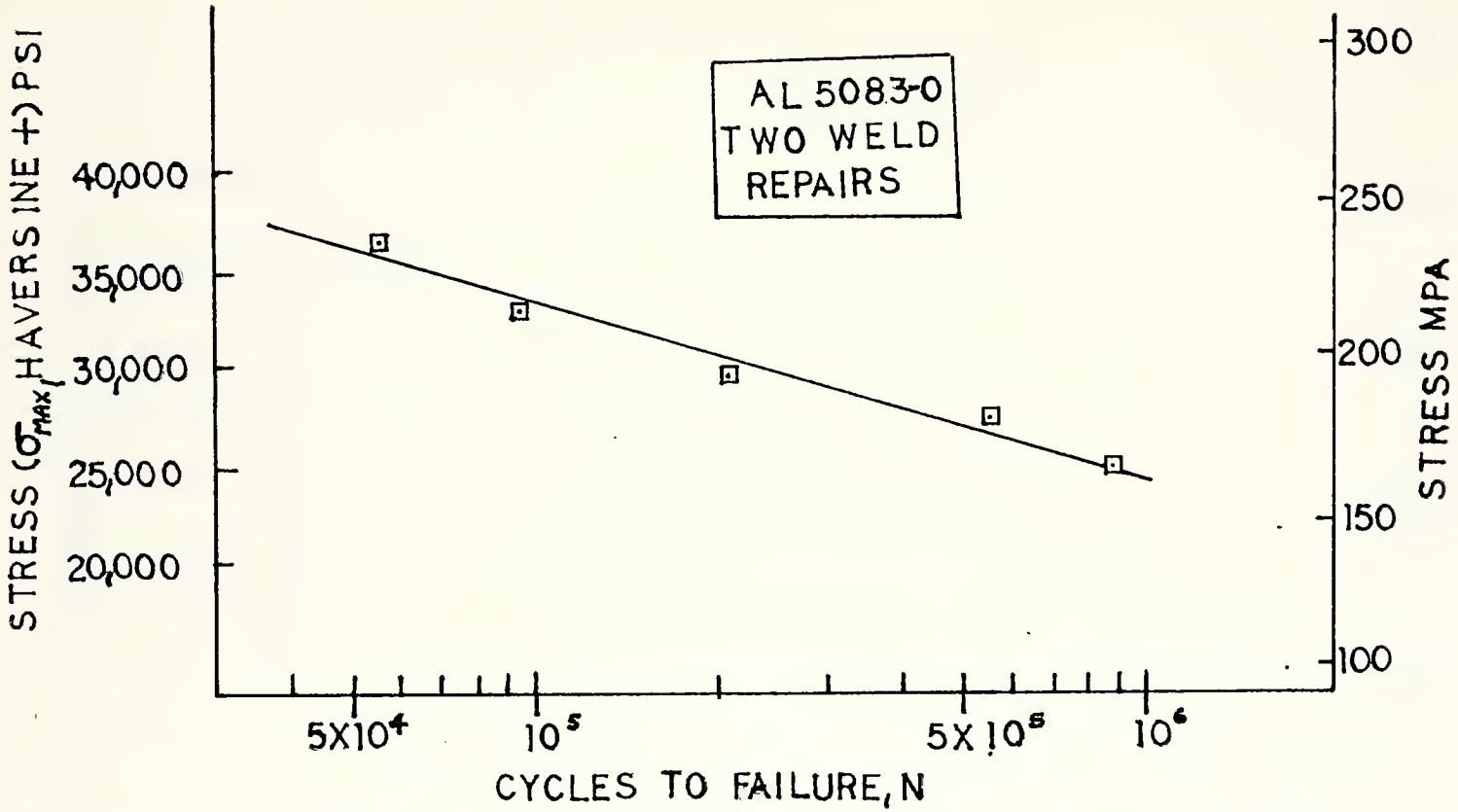

Figure 13. S-N Fatigue Diagram for AL 5083-0 which has been weld repaired twice. σ_{MAX} on the haversine loading curve is plotted on the vertical axis while cucles to failure, N, is plotted on the horizontal axis.

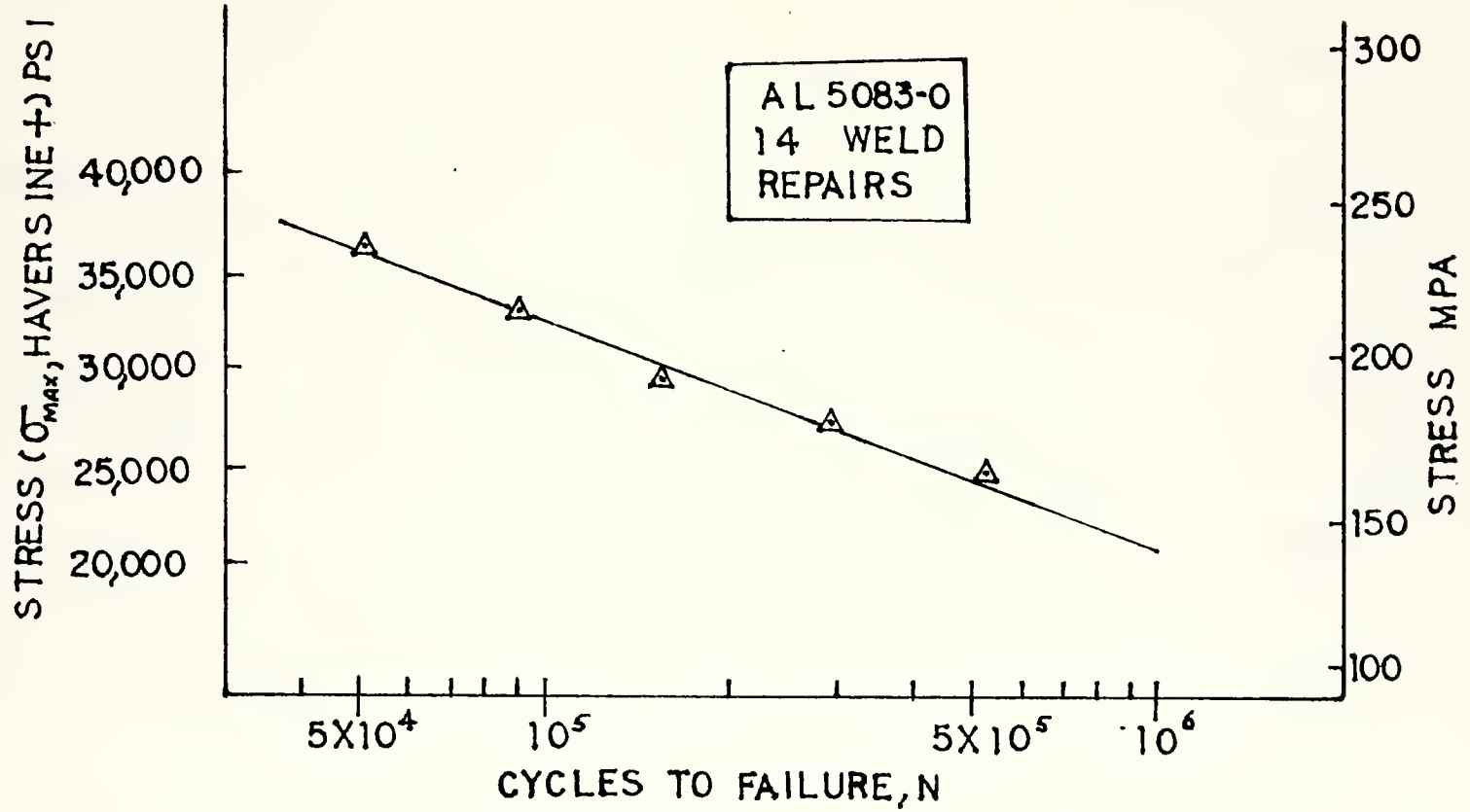

Figure 14. S-N Fatigue Diagram for AL 5083-0 which has been weld repaired fourteen times. σ_{MAX} on the haversine loading curve is plotted on the vertical axis while cycles to failure, N, is plotted on the horizontal axis.

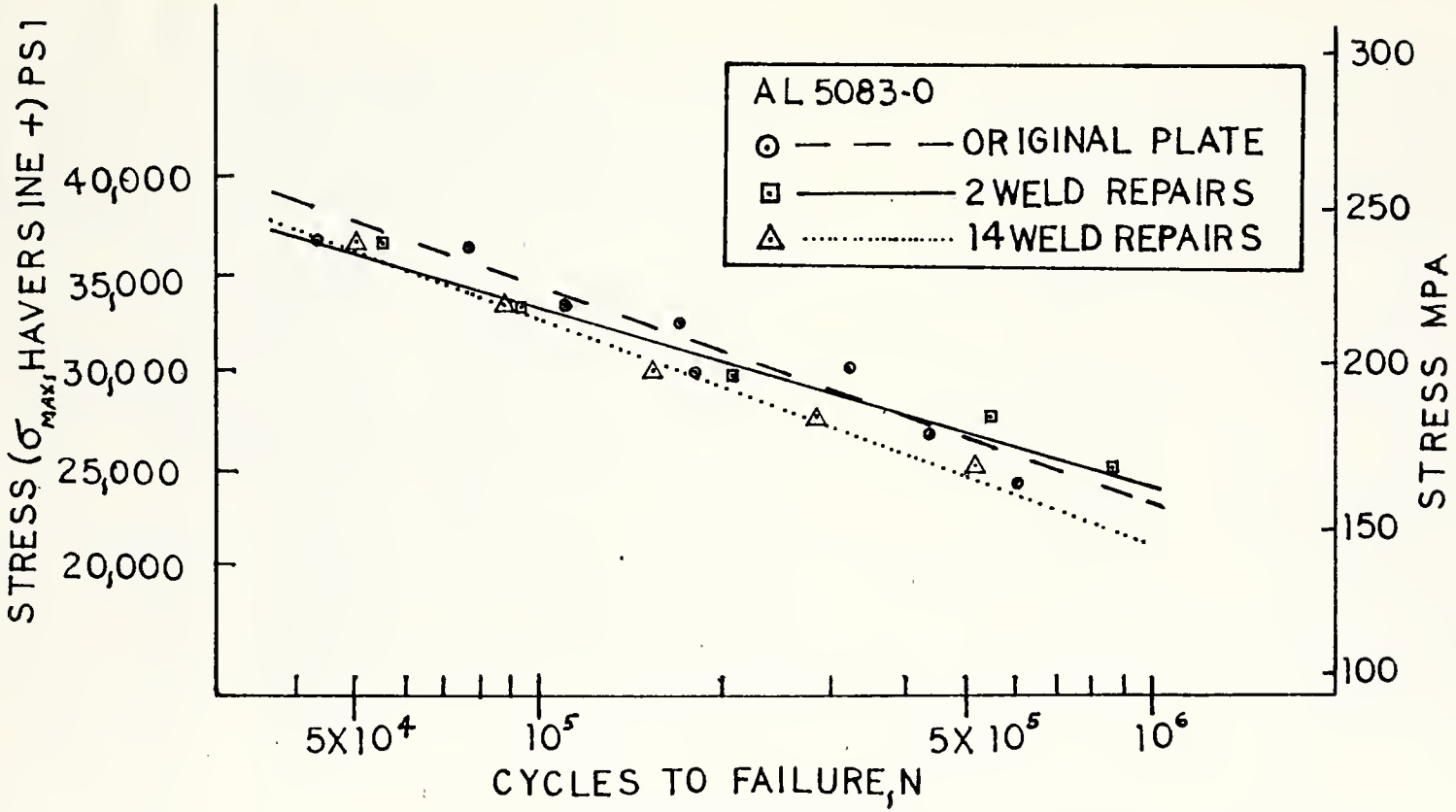

Figure 15. Comparative S-N Fatigue Diagram with Al 5083-0 original plate, two weld repaired Al 5083-0 alloy and fourteen weld repaired alloy plotted. σ_{MAX} on the haversine loading curve is plotted on the vertical axis while cycles to failure, N, is plotted on the horizontal axis.

C. SCANNING ELECTRON MICROSCOPE FRACTOGRAPHY

Scanning electron microscopy was used to study the fatigue fractures. Figure 16 is fractograph of the fracture surface of a twice weld-repaired specimen. The fatigue failure seems to proceed outward from porosity. This porosity is then the failure initiation site. Figure 17 illustrates the ductile nature of the overlaod; a classic dimple pattern is apparent on the surface.

Figures 18 and 19 illustrate a fatigue failure in an unwelded specimen. The fatigue crack apparently initiated in the upper right hand corner of the sample and proceeded inward rapidly. Fatigue beach marks are clearly evident running from the upper left to the lower right hand corner of the photographs.

Figure 20 illustrates the transverse section of the fracture surface on an unwelded sample. Figure 21, on the other hand, shows a similar transverse section of a fourteen weld repaired sample. Note that porosity is evident near the fracture surface in the weld-repaired sample. It appears that final fracture links several pores in the weld filler material. (Figure 20).

Figure 22 is the entire fracture surface of a fourteen weld-repaired sample. A large ductile overload zone and porosity on this surface are evident.

The fatigue test results and fractography reported here represent testing conducted under high-stress conditions. Extension of this data to lower stresses (and longer lifetimes) was not conducted due to time constraints. There still

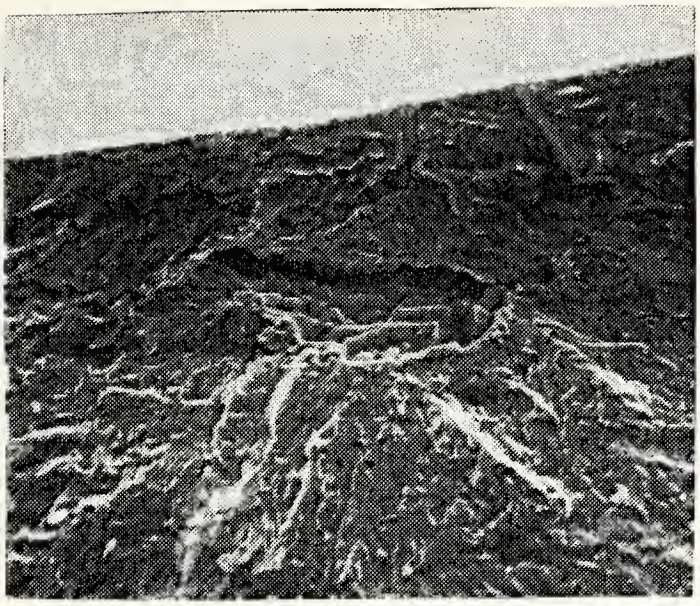

Figure 16. Observation of the fracture surface of a twice repaired specimen. (240X). The fracture appears to have initiated at porosity near the surface. Radial fatigue striations mark the progress of the fatigue crack growth.

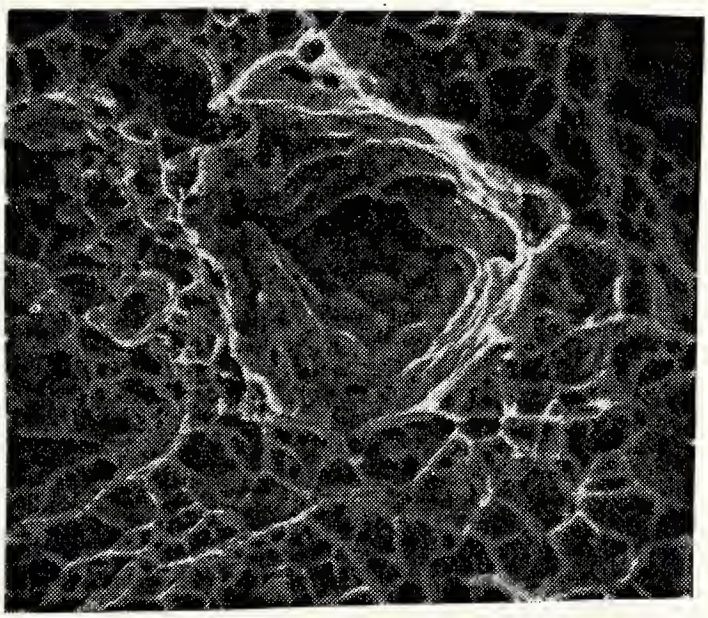

Figure 17. Observation of the fracture surface of a fourteen weld repaired sample. (620X). Porosity in the ductile overload zone is shown.

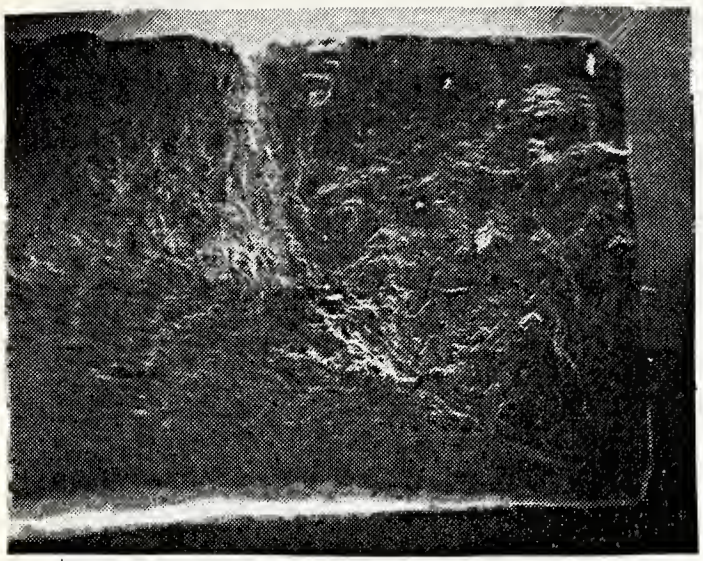

Figure 18. Observation of the fracture surface of a sample from the unwelded original. (25X). The fatigue crack seems to have begun at the free surface of the material and propagated inward.

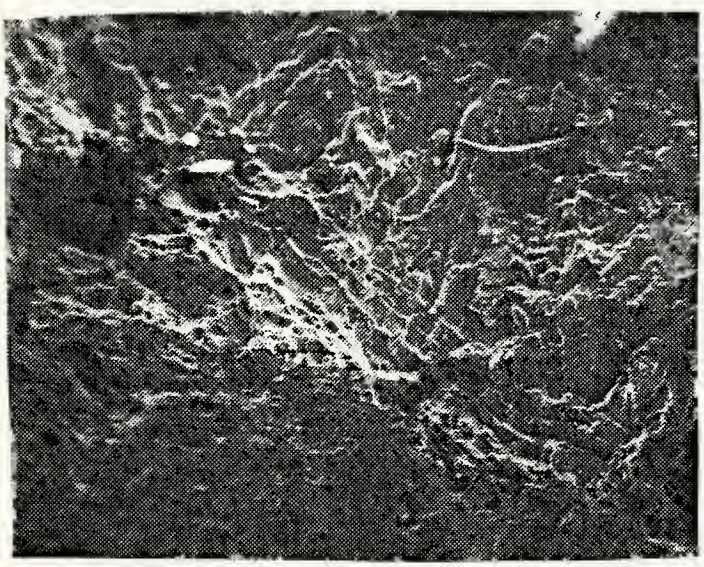

Figure 19. The fatigue zone of Figure 18 at a magnification of 51 diameters.

Figure 20. Observation of transverse section of the fracture surface. (100X). The specimen is from an original plate. Note the absence of porosity.

Figure 21. Observation of transverse section of the fracture surface of a 14 weld repaired sample. (100X). Note the porosity at or near the fracture surface. This observation along with that in Figure 12 indicate that the fatigue fracture in all welded samples was probably initiated at porosity located in the weld filler material.

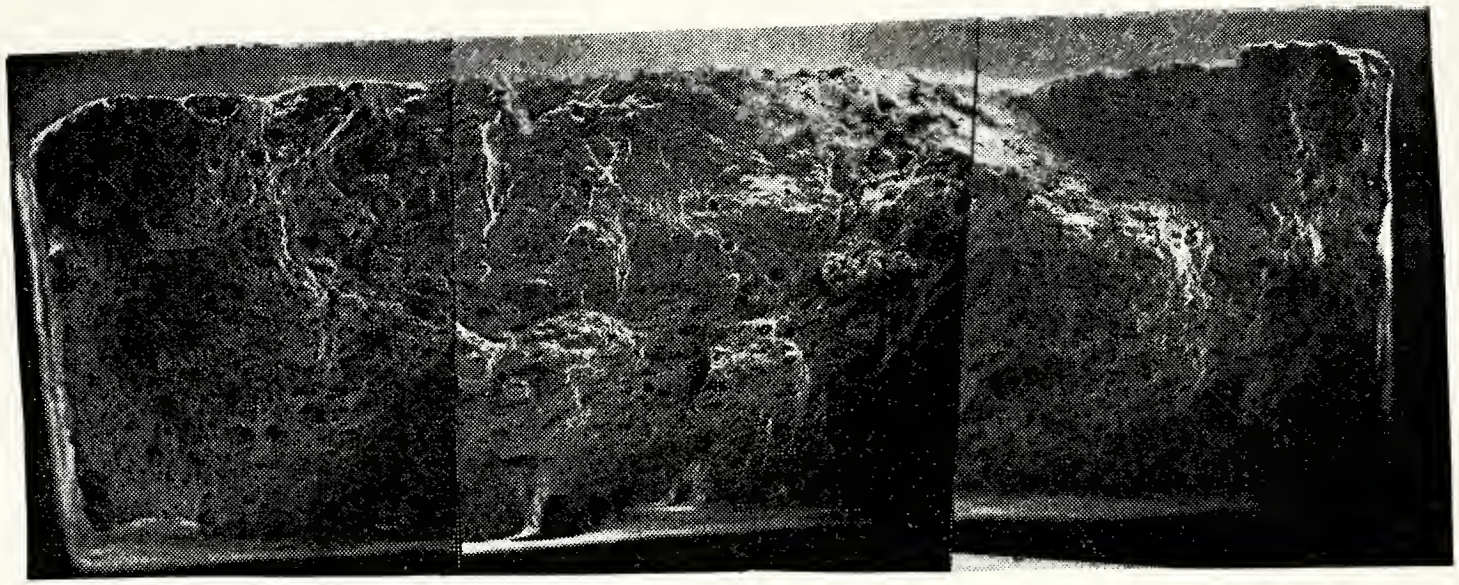

Figure 22. Observation of the entire fracture surface of a 14 weld-repaired sample. (24X). A very large ductile overload zone porosity are apparent.

remains the possibility that under low stresses the coarsened and cracked inclusions will become fatigue crack initiation sites; indeed, it is at such low stress where fatigue life in generally dominated by the crack initiation stage. It should be noted, however, that the S-N curves for twice and fourteen times repaired materials are essentially parallel betweeen 5×10^4 and 10^6 cycles to failure. Therefore, an extrapolation of these curves to higher cycles may again yield similar results.

IV. CONCLUSION

The fatigue strengths of the original AL 5083-0 plate specimen, a twice weld repaired sample and a fourteen weld repaired sample are very similar. Significantly, in the weld repaired samples failure always occurred in the weld metal. This result coupled with with similarity between the properties of the weld filler material and the original plate seem to confirm that there is little if any difference between the fatigue resistance of the three types of samples (within the inherent scatter of the fatigue testing).

Scanning electron microscopy of the fracture surfaces also verifies this result. Fatigue cracks appear to begin associated with porosity contained in the weld. Since the properties of the weld metal should remain the same despite the number of repairs, and the failure occurs in the weld, the number of weld repairs does not affect fatigue resistance.

Lt. G.R. Speight came to a similar conclusion regarding strength, hardness and stress corrosion cracking susceptibility. There was a very slight tendency toward degradation. Coupling Lt. Speight's results with those obtained in this thesis, it is possible to answer the question which was proposed in the introduction of this thesis. Multiple weld repairs do not significantly affect welded aluminum 5083-0 material properties.

LIST OF REFERENCES

1. Connors, T. G. , "Update: Domestic LNG Vessel Construction," Marine Technology, V. 15, Number 1, p. 1-13, January 1978.

2. Speight, G. R. , Jr., The Effects Of Multiple Weld Repairs On The Aluminum Alloy 5083-0, MSME Thesis, Naval Post-Graduate School, Monterey, 1978.

3. Metals Handbook, 8th ed., V. 7, p. 244, American Society For Metals, 1973.

4. Kaiser Aluminum And Chemical Sales Inc., Welding, 1967.

5. WELDING HANDBOOK, 7th ed., V. 1, p. 35-99, American Welding Society, 1976.

6. Forsyth, P. J. , The Physical Basis Of Metal Fatigue, p. 61-65, American Elsevier Publishing Company, Inc., 1969.

7. Hertzberg, R. W., Deformation And Fracture Mechanics Of Engineering Materials, p. 421-460, John Wiley and Sons, 1976.

8. Little, R. E. and Jeve, E. H., Statistical Design Of Fatigue Experiments, 1st ed., John Wiley and Sons, 1975.

9. 1978 Annual Book Of ASTM Standards, Part 10, p. 546-551, American Society For Testing And Materials, 1978.

10. Society Of Automotive Engineers, Inc., Report 790461, Fatigue Properties Of Cold-Rolled Sheet Steel, by A. R. Krause, R. W. Landgraf, and B. T. Crandall, p. 1-10, 2 March 1979.

11. Handbook Of Fatigue Testing, 1st ed., p. 19-27, American Society For Testing And Materials, 1974.

INITIAL DISTRIBUTION LIST

	No. Copies
1. Defense Technical Information Center Cameron Station Alexandria, Va. 22314	2
2. Library, Code 0142 Naval Postgraduate School Monterey, California 93940	2
3. Department Chairman, Code 69Mx Department of Mechanical Engineering Naval Postgraduate School Monterey, California 93940	1
4. Associate Professor T.R. McNelley, Code 69Mc Department of Mechanical Engineering Naval Postgraduate School Monterey, California 93940	5
5. LT. George R. Speight, Jr., U.S.C.G. Commander (mmt) Eighth Coast Guard District New Orleans, La. 70130	3
6. Commandant (G-PTE-1/72) United States Coast Guard Washington, D.C. 20590	2
7. CAPT W. D. Markle, U. S. C. G. Commandant (G-M/S2) United States Coast Guard Washington, D.C. 20590	1
8. LCDR Paul Pluta, U. S. C. G. Commandant (G-MMT-2/82) United States Coast Guard Washington, D.C. 20590	1
9. CAPT R. A. Janeck, U. S. C. G. Commandant (G-WLE/73) United States Coast Guard Washington, D.C. 20590	1
10. LCDR John R. Panico 14 Richmond Place Commack, N.Y. 11725	3

Thesis
P14575 Panico 186718
c.1
The effect of multiple weld repairs on the fatigue resistance of welded aluminum alloy 5083-0.